# Spatial and temporal changes in choroid morphology associated with long-duration spaceflight

**Charles Bélanger Nzakimuena**[1], **Marissé Masís Solano**[1, 2], **Rémy Marcotte-Collard**[3], **Mark Richard Lesk**[1, 2], **and Santiago Costantino**[1, 2,✉]

[1]Centre de Recherche de l'Hôpital Maisonneuve-Rosemont, Montréal, Québec, H1T 2M4, Canada; [2]Département d'ophtalmologie, Faculté de Médecine, Université de Montréal, Montréal, Québec, H3T 1J4, Canada; [3]École d'optométrie, Université de Montréal, Montréal, Québec, H3T 1P1, Canada

**Purpose** The development of neuro-ophthalmic symptoms during long-duration spaceflight presents major risks to astronauts and their missions. Amid efforts to understand spaceflight associated neuro-ocular syndrome (SANS), uncovering the role of the choroid in its etiology is challenged by the accuracy of image segmentation. The present study extends deep learning-based choroid quantification from optical coherence tomography (OCT) to the characterization of pulsatile and topological changes in the macular plane and investigates changes in response to prolonged microgravity exposure.

**Methods** We analyzed OCT macular videos and volumes acquired from astronauts before, during and after long-duration spaceflight. Deep learning models were fine-tuned for choroid segmentation and combined with further image processing towards vascularity quantification. Statistical analysis was performed to determine changes in time-dependent and spatially averaged variables from preflight baseline for OCT data.

**Results** For 13 astronauts with a mean age of 47 $\pm$ 9 years, there were significant increases in choroid thickness (CT) and luminal area (LA) of 14 $\pm$ 25 µm (P = 0.01) and 0.11 $\pm$ 0.2 mm$^2$ (P = 0.009) and no significant change in choroid vascularity index (CVI) averaged over OCT macular video segments. There was no significant change in the amplitude of pulsatile CT fluctuation ($\Delta$CT), but significant increases in both pulsatile LA ($\Delta$LA) and CVI ($\Delta$CVI) of 0.077 $\pm$ 0.14 mm$^2$ (P = 0.009) and 0.03 $\pm$ 0.06 (P = 0.01), respectively. For a subgroup of 6 astronauts for which inflight imaging was available, choroid volume, luminal volume and CVI over the macular region all increased significantly during spaceflight with the greatest differences reached at 90 days following launch.

**Conclusions** The findings show that localized choroid pulsatile changes occur following prolonged microgravity exposure. They suggest that the choroid vessels expand in a manner similar to the choroid layer across the macular region during spaceflight, accompanied by a relative increase in the space they occupy. The methods developed provide new tools and avenues for studying and establishing effective countermeasures to risks associated with long-duration spaceflight.

**optical coherence tomography | choroid | deep learning | spaceflight associated neuro-ocular syndrome | microgravity**

**Correspondence:** ***santiago.costantino@umontreal.ca***

## Introduction

Following prolonged exposure to microgravity, astronauts present with distinct neuro-ophthalmic findings collectively referred to as spaceflight associated neuro-ocular syndrome (SANS)[21; 26]. The symptoms defining SANS comprise unilateral and bilateral optic disc edema, posterior globe flattening, choroidal and retinal folds, hyperopic refractive error shifts, retina nerve fiber layer thickening and infarcts and increased cerebrospinal fluid volume in optic nerve sheaths[12; 13; 28; 14; 21; 26]. Depending on its severity, optic disc edema may result in permanent vision loss, and it has been identified has the chief risk associated with SANS[28]. Choroidal tissue undergoes acute variations in space over time[25], and finite element modelling of the posterior layers of the eye suggests that increased pulsatile choroid volume fluctuation may elevate strains in prelaminar neural tissue. The increased strains could in turn lead to the development of edema[4; 26].

Pulsatile choroid volume fluctuation has been used to compute ocular rigidity and evaluate its response to long-duration spaceflight[34]. The effect of microgravity exposure on pulsatile choroid volume fluctuation itself has not yet been scrutinized. However, there is evidence that the choroid expands as soon as it is exposed to microgravity[33; 17; 26], and the peripapillary choroid remains thicker than the pre-spaceflight baseline for at least 30 days and up to 90 days after landing[17; 26]. The view that choroidal swelling may be in part responsible for the hyperopic shifts and choroidal folds observed in SANS[19; 12; 13; 14], and the possible link between altered choroid pulsatility and edema warrant seeking a refined characterization of choroidal changes in response to microgravity.

The development of optical coherence tomography (OCT) with enhanced depth imaging has made possible the visualization of details of the choroid in most imaged subjects[25] and enabled the performance of reproducible biometric measurements[39; 25; 11]. Several

means of quantifying the morphology of the choroid from OCT representations have been devised[31]. Albeit routinely resorted to in clinical research contexts, manual segmentation of the choroid is labor-intensive[35; 41; 42] and ill-suited to the considerable volume of data produced by OCT devices, entailing a pace vastly exceeded by recent automated approaches[41]. The automated choroid semantic segmentation landscape has evolved from the use of various classical image processing methods[2; 22] to the application of deep neural networks[42]. Under the supervised deep learning paradigm, the transformer architecture has demonstrated superior capabilities compared to convolutional neural networks (CNNs) when applied to computer vision tasks including segmentation[27; 36].

Within the context of choroid segmentation, a few methods enable the differentiation of vasculature lumen and walls. It is now possible to identify, within a single OCT B-scan, the luminal area (LA) and to calculate choroidal vascularity index (CVI), defined as the fraction of LA over the total choroid area. However, the successful application of such parameters is highly dependent upon the accurate delineation of the choroid[1].

In the present work, we train deep learning models to reliably produce choroid semantic segmentations in macular images from OCT videos and OCT volumes acquired from astronauts. We complement our segmentation techniques with vascularity quantification, enhancing the ability to characterize the state of the choroid and its variations. We extend the capability of our approaches to OCT image timeseries and OCT volume reconstructions. For video acquisitions, we compare pre- and post-spaceflight quantifications and reveal significant changes in time-dependant variables. For volumes, we capture substantial mapping changes over several timepoints in a cohort of astronauts exposed to microgravity.

# Methods

### Datasets

The study was approved by the institutional review boards of the Maisonneuve-Rosemont hospital and NASA, and the clinical research ethics committee of Université de Montréal. The study was conducted according to the Declaration of Helsinki and its amendment. Two datasets were used (see table S1 for a summary). All acquisitions were performed using spectral-domain OCT (Spectralis OCT2; Heidelberg Engineering, Heidelberg, Germany). There was no pathology reported in any of the subjects participating in the study.

OCT macular videos were acquired pre- and post-spaceflight from both eyes, with up to 5 videos per eye at each timepoint. Each frame has dimensions 768 × 496 pixels, approximately corresponding to 8.4 × 1.9 mm, and each video is roughly 1 minute in length. A resting heart rate measurement was also obtained concurrently with video acquisition.

For the analysis of changes in 3-dimensional topology due to microgravity exposure, we used a set of OCT macular volumes composed of 97 or 193 B-scans. The macula block setting was used with placement over the fovea via the anatomic positioning system for each acquisition. For each timepoint, up to 2 volumes per eye were obtained. All frames in the set of OCT macular volumes measure 512 × 496 pixels, which physically approximates to 5.6 × 1.9 mm.

### Segmentation performance evaluation

SegFormer models[40] pretrained on the ImageNet database were retrained directly on both datasets towards choroid segmentation. For OCT videos, training data was gathered by randomly selecting 10 B-scans per movie where the choroid region was manually labelled by one trained grader and binarized. To implement 5-folds cross-validation, the training data was arranged 5 different ways, in each instance splitting the whole into training, validation and test sets. For each fold, 10 % of B-scans were assigned to the validation set, and 10 % to the test set. The training and validation sets were used for model training and the test sets were used for performance evaluation.

For OCT volumes, we devised a strategy to ensure adequate representation of the distribution of B-scans corresponding to each subject's eye in the training data. The image set was split into 5 groups along the slow acquisition direction, and 4 B-scans from each group were randomly selected for a total of 20 per volume. For each volume, 4 B-scans out of 20 were manually labelled by one trained grader and binarized. The locations of the labelled B-scans were subsequently shifted as shown in figure S7. Training data 5-folds cross-validation was then implemented in the same manner as described for videos.

Post-processing was implemented to ensure continuous layer boundaries and minimize the effect of isolated false positive regions (details are provided in Supplementary Information B). The test set 5-fold cross-validation performance for both the videos and volumes datasets was evaluated based on similarity metrics, as well as choroid boundaries mean absolute error (MAE) and choroid thickness difference (TD) between the manually segmented and corresponding automatically segmented frames. The equations for MAE and TD are provided below

$$MAE = \frac{1}{m}\sum_{i=1}^{m}\left|y^{(i)} - \hat{y}^{(i)}\right| \quad \textbf{(1)}$$

$$TD = \frac{1}{m}\sum_{i=1}^{m}\left|\left|y^{(i)}_{CSI} - y^{(i)}_{BM}\right| - \left|\hat{y}^{(i)}_{CSI} - \hat{y}^{(i)}_{BM}\right|\right| \quad \textbf{(2)}$$

where m is the B-scan width and $y^{(i)}$ and $\hat{y}^{(i)}$ are the inferred and manually labeled vertical boundaries of Bruch's membrane (BM) or the choroid-sclera interface (CSI). Sørensen–Dice coefficient complement ($Dice^C$)

and Jaccard coefficient complement (Jaccard$^C$) were used as similarity metrics. We also defined mathematical expressions to identify inaccurate segmentation and segmentation failure associated with subtle and gross segmented boundary aberrations, respectively (equations are provided in Supplementary Information C).

Beyond choroid segmentation, we produced masks of LA to calculate CVI (details are provided in Supplementary Information D). CVI was calculated as LA divided by total choroid layer area. The LA processing performance was assessed on the test set of selected SegFormer models for both videos and volumes using similar methods as for choroid segmentation performance evaluation. Additional test set performance evaluations relating to choroid layer and lumen segmentation are provided in Supplementary Information H.

### Temporal analysis

Inference was only performed on B-scans which met noise specifications based on OCT device manufacturer defined metrics. Specifically, only B-scans with a quality score equal to or greater than 24 (0-40 score range; 0 indicating no signal and 40 indicating excellent quality) and with an automatic real time frame averaging number greater or equal to 2 were considered. The automatic real time averaging setting was 3 frames per B-scan.

B-scans with a signal-to-noise ratio beneath 0.55 were also excluded. The signal-to-noise ratio equation used is provided below

$$SNR = \frac{S}{\sigma} \quad \textbf{(3)}$$

where SNR is the signal-to-noise ratio, S is the mean and $\sigma$ is the standard deviation of the intensities in a B-scan. B-scans for which the inferred choroid region was located within 10 % of the superior or inferior vertical edge of the image were excluded. Single B-scans with an inferred choroid area (CA) departing from the average of the manually segmented frames by greater or equal to 20 % were also excluded.

OCT videos were unevenly sampled and frequency analysis was performed with Lomb–Scargle periodograms and spectrograms generated over a 0.1-4 Hz frequency range (transforms implementation details and calibration test results are provided in Supplementary Information F). Movies with less than 50 good quality frames were discarded. To prevent large gaps in a video, we preserved only the longest video segment for which no zone of excluded frames amounting to greater than 1 s was present. Pulsatile CT, LA and CVI ($\Delta$CT, $\Delta$LA, $\Delta$CVI) were computed as done by Beaton et al[2]. First, the locations of peaks and valleys across time series were obtained, where the minimum distance between them is given by the expression

$$d_{min} = \frac{T_{heart}}{3 \cdot M_{o,\ intervals}} \quad \textbf{(4)}$$

where $d_{min}$ is the minimum distance between peaks and between valleys, $T_{heart}$ is the heart period and $M_{o,\ intervals}$ is the mode of the 1D array of intervals between each element in a time series. Having obtained peaks and valleys locations, consecutive peaks between valleys and consecutive valleys between peaks were discarded. $\Delta$CT, $\Delta$LA and $\Delta$CVI were then defined as the difference between the median of all remaining peaks and the median of all remaining valleys.

Linear mixed models were used to determine statistical significance of choroid quantification differences pre- and post-spaceflight. For each linear mixed model, timepoints were designated as the fixed effect. Subjects and eyes nested under each subject were specified as random effects[3]. Significance values were gathered using the Kenward-Roger approximation[16].

### Spatial analysis

For OCT volumes, the automatic real time averaging setting was 15 frames per B-scan. Following initial segmentation, smoothing of the surface of the CSI across each macular volume was implemented using a graph search algorithm similar to the one described by Mazzaferri et al[22]. The graph search algorithm was applied to each one of the volume's cross-sectional image along the fast acquisition direction.

Having delineated the region between the BM and a smoothed CSI, choroid volume (CV), luminal volume (LV) and CVI were quantified (CT and LT are included in Supplementary Information K). In addition to a global level value, the result of each quantification was split into macular ETDRS subfields (center; superior inner; nasal inner; inferior inner; temporal inner; superior outer; nasal outer; inferior outer; temporal outer).

For better visualization, we created square maps of CT, LT and CVI of 512 × 512 pixels by interpolating the total number of B-scans of every OCT volume and we analysed variation across timepoints. Linear mixed models were used to determine statistical significance between timepoints. The same specifications were used to implement the linear mixed models as for the temporal choroid OCT data analysis.

### Loss function

The training of the SegFormer models was achieved through the IoU loss. For binary segmentation, which was used exclusively in the present study, the IoU loss equation is given by

$$\mathcal{L}_{IoU} = 1 - \frac{\sum_{i=1}^{N} g_i s_i}{\sum_{i=1}^{N} (g_i + s_i - g_i s_i)} \quad \textbf{(5)}$$

where $\mathcal{L}_{IoU}$ is the IoU loss, N is the number of pixels in an image, $s_i$ is the predicted value of the $i^{th}$ pixel in an image, and $g_i$ is the targeted ground truth value of the $i^{th}$ pixel in an image.

### Training process

The SegFormer models were trained using the Adam optimizer. A 0.0001 learning rate was used as well as early stopping based on validation loss for both SegFormer models. No data augmentation strategy was carried as part of training the SegFormer models.

All training was implemented on a Windows 11 computer equipped with a NVIDIA GeForce RTX 2060 Graphics Processing Unit (GPU). Training of the SegFormer transformer models was completed on Python (v3.10.0) using PyTorch Lightning (1.8.6).

## Results

### SegFormer-based choroid segmentation

We sought to quantify choroid morphology changes in response to microgravity exposure. For this, we retrained SegFormer models directly on astronaut OCT macular videos and volumes and implemented a simple post-processing strategy to analyze vascular changes. We manually labeled a subset of images representing 2 % of available images and assessed the test set performance of the pipeline using different metrics.

We leveraged a dataset of OCT macular videos to compare pre- and post-spaceflight time-dependant variables obtained from astronauts. We used images centered at the macula from 13 individuals, 9 male and 4 female of average age 47 $\pm$ 9 yo. There were 8 astronauts who did not have prior spaceflight experience, 3 who had completed Space Shuttle short-duration missions, and 4 who had previous long-duration spaceflight experience ($>$ 4 months[15]). All preflight videos were obtained within a 9 to 1 month before spaceflight window and all postflight videos within 2 to 30 days after spaceflight.

Figure 1a and b display illustrations of 3 individuals' manual and automated segmentations showing excellent correspondence for both choroid and vascular lumen obtained from OCT videos. Mean Dice$^C$ and mean Jaccard$^C$ for the OCT videos test set (figure 1c) were 0.044 $\pm$ 0.02 and 0.083 $\pm$ 0.03, respectively. Figure 1d provides segmentation mean absolute error (MAE), expressed as the deviation of the boundary (in pixel units) from the labeled traces. It also shows thickness difference (TD) which represents the deviation of the layer thickness (in pixels) from the labeled layer. Test set BM and CSI MAE were 0.93 $\pm$ 0.3 pixels and 6.2 $\pm$ 2.7 pixels, respectively, and TD was 6.1 $\pm$ 2.7 pixels. Test set LA mean Dice$^C$ and mean Jaccard$^C$ were 0.32 $\pm$ 0.1 and 0.48 $\pm$ 0.09, respectively (figure 1e).

The performance was similar for the B-Scans from OCT volumes (manual and automated segmentations are shown in figure 1f and g). This second set contains OCT volumes centered at the macula from 6 of the 13 astronauts featured in on-Earth videos, 5 males and 1 female, which were of average age 48 $\pm$ 9 yo. There were 4 astronauts who did not have prior spaceflight experience, 1 who had completed Space Shuttle short-duration missions, and 2 who had previous long-duration spaceflight experience. The volumes were obtained at up to 6 different timepoints before launch (launch - 21 to 18 months, launch - 9 to 6 months), during flight and before return (launch + 30 days, launch + 90 days, return - 30 days) and following spaceflight (return + 1 to 3 days). Test set choroid segmentation mean Dice$^C$ and mean Jaccard$^C$ for OCT macular volumes were 0.057 $\pm$ 0.02 and 0.11 $\pm$ 0.04, respectively (figure 1h). Test set BM and CSI MAE for the same fold were 1.2 $\pm$ 0.3 pixels and 8 $\pm$ 4.2 pixels, respectively, and TD was 7.9 $\pm$ 3.9 pixels (figure 1i). Test set LA mean Dice$^C$ and mean Jaccard$^C$ were 0.39 $\pm$ 0.07 and 0.55 $\pm$ 0.07, respectively (figure 1j). Additional choroid layer segmentation and lumen segmentation performance evaluations are provided in supplementary figures S8 and S9.

### Quantification of choroid pulsatile changes

We investigated the presence of spaceflight-related changes in choroid pulsatility. For this, as we have done in the past[2], we obtained videos of OCT images of about 1 minute, acquired at 14 Hz. The built-in eye tracker of the OCT device was used to assure that the same location in the macula was sampled throughout the video. The acquisition was automatically halted when a patient moved, only resuming after the laser was repositioned. Our choroid quantification approaches were implemented on the videos, yielding timeseries which displayed morphological changes at the frequency of the heart. Because images are not sampled at a constant rate, Lomb–Scargle periodograms and spectrograms of normalized power were expected to show peaks in the heart rate vicinity. Detection of those peaks, as illustrated in figure 2g-i, serves as quality control for segmentation. Narrow and prominent maxima can often be seen for CT, LA and CVI (also figures S11 and S12, second and third columns).

We found a global CT averaged over movie durations significant increase of 14 $\pm$ 25 µm or 4.7 % (linear mixed model, P = 0.01) from pre- to postflight, and global LA significant increase of 0.11 $\pm$ 0.2 mm$^2$ or 6.8 % (linear mixed model, P = 0.009) (figure 2a and b), but no change in global CVI (figure 2c). For the analysis of the amplitude of pulsatile fluctuations, no significant differences in $\Delta$CT were found globally (figure 2d). As shown in figure 2e and f, both global $\Delta$LA and $\Delta$CVI did show significant increases from pre- to postflight of 0.077 $\pm$ 0.14 mm$^2$ or 34 % (linear mixed model, P = 0.009) and 0.03 $\pm$ 0.06 or 35 % (linear mixed model, P = 0.01), respectively. We provide baseline pre-spaceflight results of our choroid quantification methods for OCT videos from astronaut eyes, including their ETDRS subfield equivalents in supplementary table S2. The ETDRS subfield equivalents of the measures displayed in figure 2a-f are provided in supplementary figure S10,

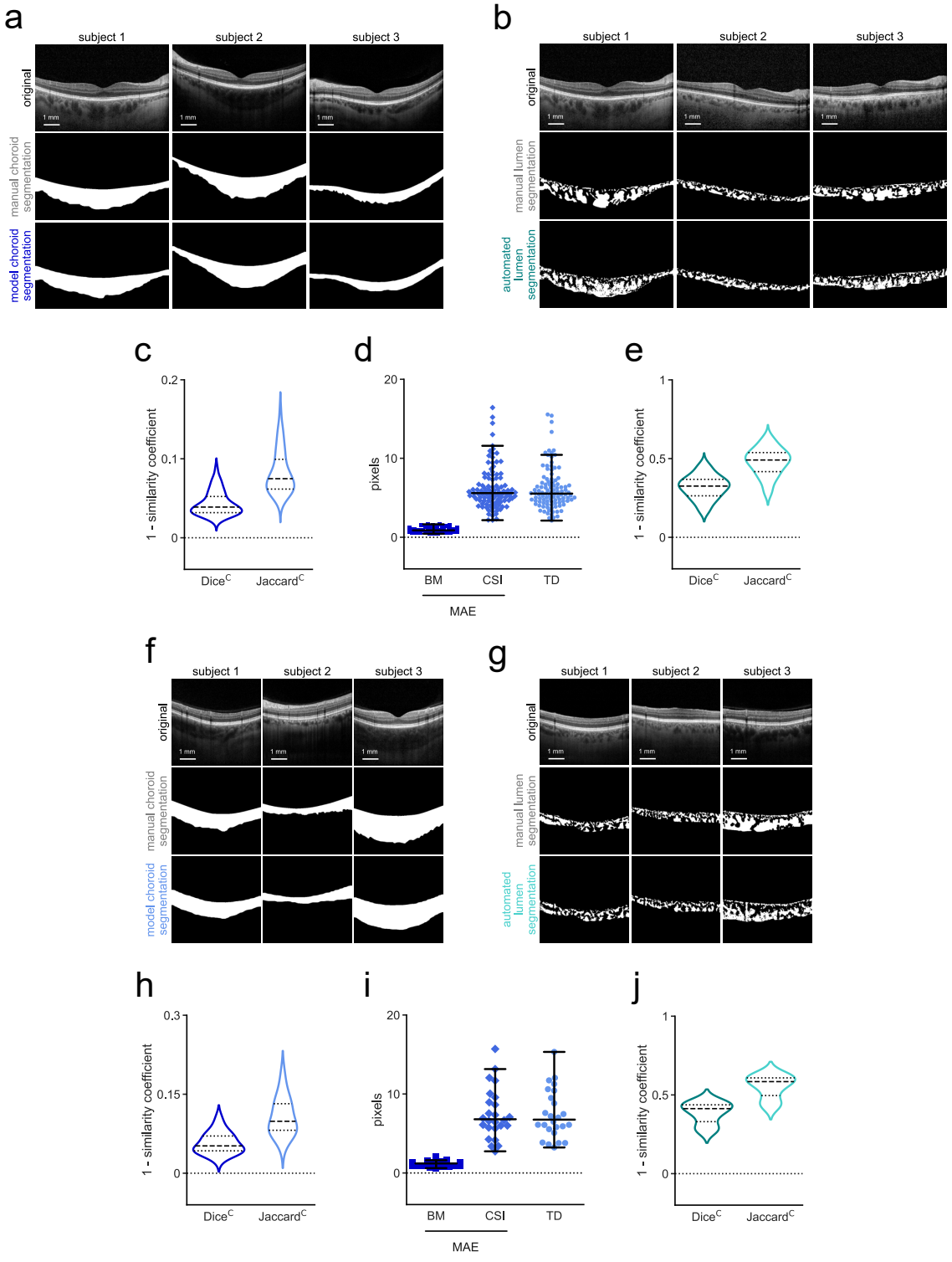


**Figure 1. Choroid layer and lumen segmentation performance evaluation.** (**a**) Original OCT video B-scans and binary choroid layer segmentation masks for 3 subjects obtained manually and through model inference. (**b**) Original OCT video B-scans and binary lumen segmentation masks for 3 subjects obtained manually and automatically. (**c**) Violin plots displaying test set Dice$^C$ and Jaccard$^C$ between manual and model choroid layer segmentations for OCT videos. (**d**) Swarm plots of test set BM and CSI mean absolute errors and average choroid thickness difference between manual and model choroid layer segmentations for OCT videos. (**e**) Violin plots displaying test set Dice$^C$ and Jaccard$^C$ between manual and automated lumen segmentations for OCT videos. (**f**) Original OCT volume B-scans and binary choroid layer segmentation masks for 3 subjects obtained manually and through model inference. (**g**) Original OCT volume B-scans and binary lumen segmentation masks for 3 subjects obtained manually and automatically. (**h**) Violin plots displaying test set Dice$^C$ and Jaccard$^C$ between manual and model choroid layer segmentations for OCT volumes. (**i**) Swarm plots of test set BM and CSI mean absolute errors and average choroid thickness difference between manual and model choroid layer segmentations for OCT volumes. (**j**) Violin plots displaying test set Dice$^C$ and Jaccard$^C$ between manual and automated lumen segmentations for OCT volumes.

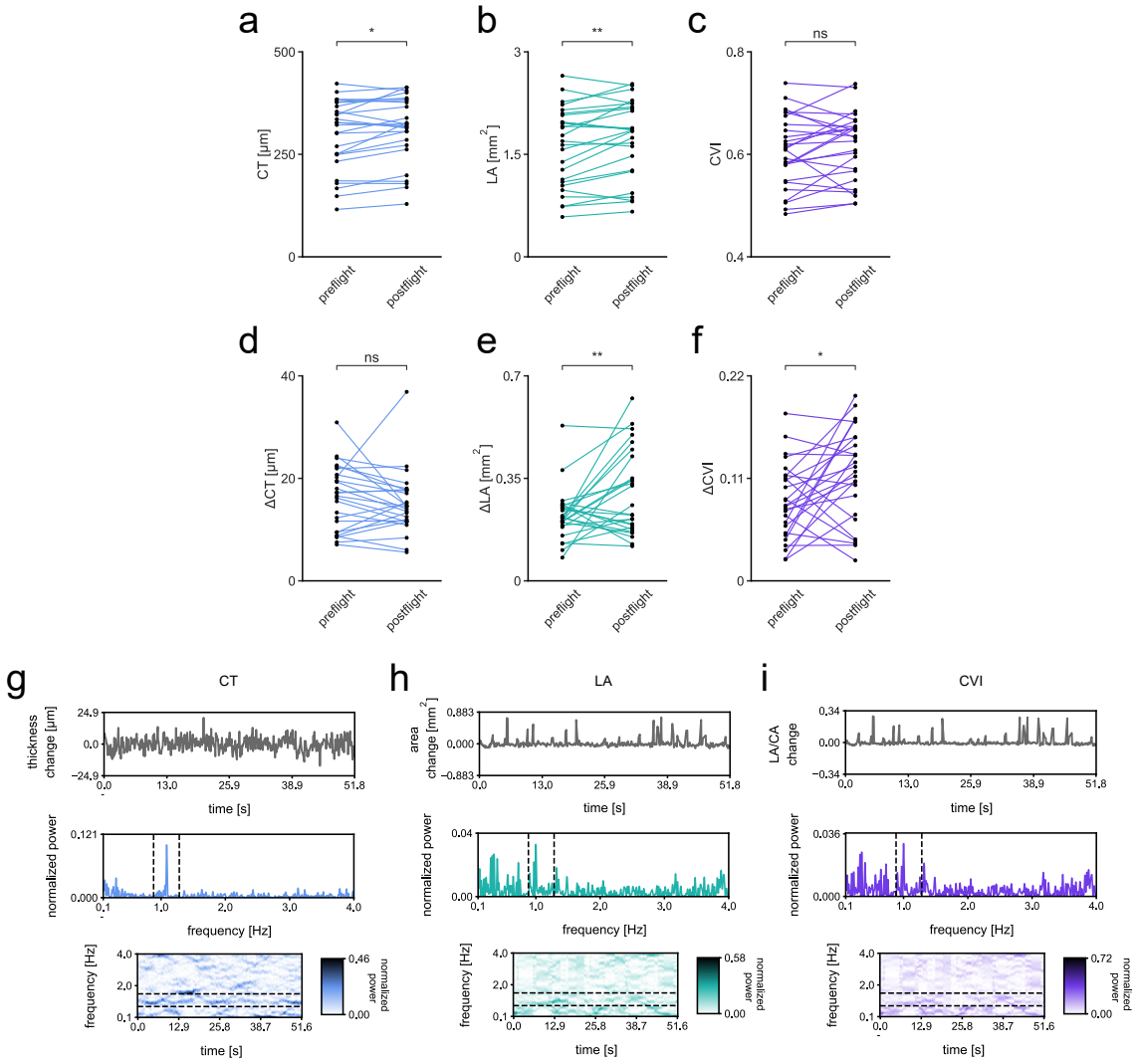


**Figure 2. Temporal OCT spaceflight-related choroid pulsatile changes and choroid pulse detection.** (**a**) Paired line plot comparing post- and preflight CT measurements averaged over the selected segments for all astronaut eyes. (**b**) Paired line plot comparing post- and preflight LA measurements. (**c**) Paired line plot comparing post- and preflight CVI measurements. (**d**) Paired line plot comparing post- and preflight $\Delta$CT measurements corresponding to the selected segment. (**e**) Paired line plot comparing post- and preflight $\Delta$LA measurements. (**f**) Paired line plot comparing post- and preflight $\Delta$CVI measurements. *P $<$ 0.05, **P $<$ 0.01, linear mixed model. (**g**) Selected segment CT timeseries, frequency and joint time-frequency transforms for one subject's eye acquisition. Top row features selected segment timeseries, second row features the Lomb–Scargle periodogram and third row features the Lomb–Scargle spectrogram. Dashed lines on the Lomb–Scargle periodogram and Lomb–Scargle spectrogram show values $\pm$ 20 % and $\pm$ 40 % of the oximeter measured heart rate value, respectively. (**h**) Selected segment LA timeseries, frequency and joint time-frequency transforms for the same subject. (**i**) Selected segment CVI timeseries, frequency and joint time-frequency transforms for the same subject.

and significance in table S4. Positive correlations were found between all global metrics and TRT250 but none were significant for the available data.

### Spatial choroid changes associated with long-duration spaceflight

We extended our choroid quantification techniques to OCT volumes, for which large variations were expected in astronauts. Each volume is made up of 97 or 193 B-scans. In addition to obtaining cross-sectional image segmentation performance, we generated maps exposing choroid thickness topography and vascular patterns. Choroid vessel patterns were readily observable on LT and CVI maps in OCT volumes (figure 3d). For all eyes, there was a correspondence between CT and LT maps, with thicker choroid regions generally translating to thicker luminal regions. Different degrees of retinal vessel shadow artifacts were discernable in most scans.

When comparing individual timepoints with preflight, there were significant differences for global CV and LV (figure 3a and b) for all measurements. The same comparison for global CVI measurements indicated significant differences for inflight timepoints and normal values for return + 1 to 3 days (figure 3c). We provide baseline results of our choroid quantification methods for OCT volumes from astronauts, including their ETDRS subfield equivalents in supplementary table S3.

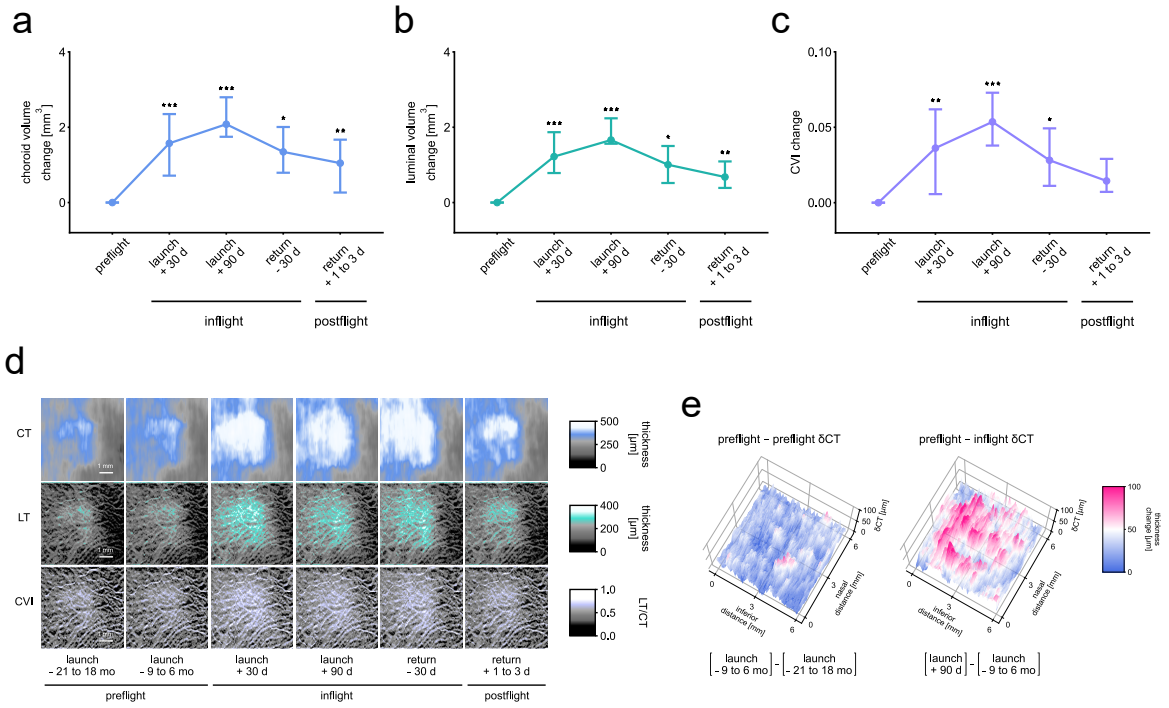


**Figure 3. Spatial OCT choroid changes associated with long-duration spaceflight.** (**a**) Line chart of change in CV over preflight, inflight and postflight timepoints for all astronaut eyes. Error bars show the difference interquartile range and dots show the mean difference. (**b**) Line chart of change in LV over preflight, inflight and postflight timepoints for the same eyes. (**c**) Line chart of change in CVI over preflight, inflight and postflight timepoints for the same eyes. (d days). *P $<$ 0.05, **P $<$ 0.01, ***P $<$ 0.001, linear mixed model. (**d**) Maps of CT, LT and CVI over preflight, inflight and postflight timepoints for one subject's eye. The top row displays CT maps, the middle row displays LT maps, and the bottom row displays CVI maps. (d days, mo months). (**e**) Surface plots of the difference between two preflight CT maps (launch - 21 to 18 months and launch - 9 to 6 months) (left), and of the difference between preflight and inflight CT maps (launch - 9 to 6 months and launch + 90 days) (right) for the same subject's eye acquisitions. ($\delta$CT choroid thickness change).

The ETDRS subfield equivalents of measures displayed in figure 3a-c are provided in Supplementary Information K, and significance values in supplementary tables S5-S8.

## Discussion

In addition to an increase in CT within the macular region during the month that follows long-duration spaceflight, we found an increase in the area corresponding to the lumen. Our results also indicate that while pulsatile fluctuation in CT did not change compared to preflight when measured within 30 days of return, the amplitude of pulsatile fluctuation in LA increases. During missions, we observed a global increase in the space occupied by lumen relative to the whole choroid layer across the macular plane.

Consistent with our results, a study which measured macular CT preflight and during spaceflight showed a 35 µm CT increase[6]. Previous reports demonstrated similar increases in peripapillary CT. Laurie et al found a mean peripapillary CT increase of 27 µm during spaceflight compared to preflight[10]. Macias et al observed progressive peripapillary choroid thickening over the course of long-duration spaceflight, with a mean increase of 43 µm at 150 days[17]. In line with our findings for CT at the macula, they also showed still significantly increased peripapillary CT at 30 days following return to Earth. Unlike the present work, previous studies were limited to measuring CT from a single image. Here we complement previous reports by adding maps of thickness change, as well as an analysis of how lumen and CVI evolve and their response to cardiac pulsation.

Several mechanisms have been proposed to account for increased CT upon microgravity exposure. They include cephalad fluid shift resulting in venous congestion and accumulation of blood in the choroid[18; 12; 14] as well as persistent buildup of choroidal interstitial fluid in the peripapillary area[38; 26]. Determining the source of optic disc edema observed in SANS has been described as challenging using available technology and approaches to data analysis[17]. Our results are in line with finite element modelling which suggested a link between choroid anatomy, increased pulsatile choroid volume fluctuation, prelaminar neural tissue strains and the development of edema[4; 26].

A mathematical model of the cardiovascular response to long-duration spaceflight predicted increased upper body blood volume[5]. Multiple authors have demonstrated that the choroid expands in weightlessness, leaving open the question of choroidal pulsatility and its possible change in weightlessness. Our study directly shows increased amplitude of pulsatile fluctuation of

the space occupied by choroid vessels after spaceflight, opening the possibility of investigating its relationship with peripapillary retinal thickness increase in SANS. Pulsatile deformation of the optic nerve head may be assessed using OCT[32] and could also be studied in relation to choroid pulsatile changes, helping substantiate finite element modelling predictions.

Studies have linked the development of edema in SANS with single nucleotide polymorphisms (SNPs)[43; 44]. A lower enzyme functional activity in the 1-carbon pathway can increase B-vitamins requirements and the risk of vitamin insufficiency[45]. Folic acid and its active metabolite, 5-methyltetrahydrofolate, maintain endothelial nitric oxide synthesis and NADPH consumption coupling. Uncoupling decreases nitric oxide synthesis and increases the generation of reactive oxygen species[8; 23]. Oxidative stress in turn increases endothelial permeability, widening interendothelial junctions and resulting in protein and fluid leakage into the interstitial space[7; 24]. The present study did not differentiate between astronauts with specific genetic profiles, but the approaches we developed could be used to determine whether individuals with SANS-relevant SNPs are more likely to show choroid layer or lumen pulsatile fluctuation changes, and whether they are more vulnerable to them.

The application of lower body negative pressure has been explored as a means of mitigating the effects of cephalad fluid shift in SANS. While lower body negative pressure was shown to decrease intraocular pressure in astronauts during spaceflight, no change in macular CT was observed[6]. Numerical modelling suggests that under microgravity conditions, less rigid vessels are subjected to increased transmural pressure and greater than normal volume[9]. An artificial gravity experiment achieved partial alleviation of mice retinal tissue damage associated with weightlessness exposure[20; 37]. The effects of artificial gravity on the state of the choroid have not been explored, and the need for precise and reliable methods of assessing SANS-related eye alterations to validate its effectiveness as a countermeasure has been emphasized[37]. The approaches we developed for the measurement of pulsatile and volume choroid changes represent a step in this direction.

The significant postflight global and localized increases in $\Delta$LA and $\Delta$CVI we observed could be associated with increased choroidal vessel compliance following sustained greater than normal volume during long-duration spaceflight. Pulsatile choroid volume fluctuation correlates inversely with the measurement of ocular rigidity performed using an invasive procedure[30]. Combined with additional measurements, our choroid layer segmentation method has the potential to improve upon a key element in the reliable, non-invasive computation of ocular rigidity[2; 29]. An early exploration of ocular rigidity in a private astronaut suggested that it decreases following spaceflight[33], and this was recently confirmed in professional astronauts[34]. Our work provides the means to build upon previous findings and further unravel the relationship between ocular rigidity and spaceflight, including its role a risk factor for developing of SANS.

## Conclusions

Neuro-ophthalmic findings in spaceflight associated neuro-ocular syndrome (SANS) including optic disc edema constitute important risks for astronauts and their missions. Weightlessness results in rapid choroidal expansion which may partially account for concerning SANS findings. Macular region luminal area and the amplitude of its pulsatile fluctuation were both increased compared to preflight within 30 days after long-duration spaceflight. During long-duration spaceflight, there is a global increase in both the choroid layer and the relative space occupied by lumen inside the choroid across the macular plane.

## References

1. Rupesh Agrawal, Jianbin Ding, Parveen Sen, Andres Rousselot, Amy Chan, Lisa Nivison-Smith, Xin Wei, Sarakshi Mahajan, Ramasamy Kim, Chitaranjan Mishra, et al. Exploring choroidal angioarchitecture in health and disease using choroidal vascularity index. *Progress in retinal and eye research*, 77:100829, 2020.
2. L Beaton, J Mazzaferri, F Lalonde, M Hidalgo-Aguirre, D Descovich, MR Lesk, and S Costantino. Non-invasive measurement of choroidal volume change and ocular rigidity through automated segmentation of high-speed oct imaging. *Biomedical optics express*, 6(5):1694–1706, 2015.
3. Qiao Fan, Yik-Ying Teo, and Seang-Mei Saw. Application of advanced statistics in ophthalmology. *Investigative ophthalmology & visual science*, 52(9):6059–6065, 2011.
4. Andrew J Feola, Emily S Nelson, Jerry Myers, C Ross Ethier, and Brian C Samuels. The impact of choroidal swelling on optic nerve head deformation. *Investigative ophthalmology & visual science*, 59(10):4172–4181, 2018.
5. Caterina Gallo, Luca Ridolfi, and Stefania Scarsoglio. Cardiovascular deconditioning during long-term spaceflight through multiscale modeling. *npj Microgravity*, 6(1):27, 2020.
6. Scott H Greenwald, Brandon R Macias, Stuart MC Lee, Karina Marshall-Goebel, Douglas J Ebert, John HK Liu, Robert J Ploutz-Snyder, Irina V Alferova, Scott A Dulchavsky, Alan R Hargens, et al. Intraocular pressure and choroidal thickness respond differently to lower body negative pressure during spaceflight. *Journal of Applied Physiology*, 131 (2):613–620, 2021.
7. Hadi AR Hadi, Cornelia S Carr, and Jassim Al Suwaidi. Endothelial dysfunction: cardiovascular risk factors, therapy, and outcome. *Vascular health and risk management*, 1(3):183–198, 2005.
8. Zvonimir S Katusic. Vascular endothelial dysfunction: does tetrahydrobiopterin play a role? *American Journal of Physiology-Heart and Circulatory Physiology*, 281(3):H981–H986, 2001.
9. Mimi Lan, Scott D Phillips, Veronique Archambault-Leger, Ariane B Chepko, Rongfei Lu, Allison P Anderson, Kseniya S Masterova, Abigail M Fellows, Ryan J Halter, and Jay C Buckey. Proposed mechanism for reduced jugular vein flow in microgravity. *Physiological Reports*, 9(8):e14782, 2021.
10. Steven S Laurie, Stuart MC Lee, Brandon R Macias, Nimesh Patel, Claudia Stern, Millennia Young, and Michael B Stenger. Optic disc edema and choroidal engorgement in astronauts during spaceflight and individuals exposed to bed rest. *JAMA ophthalmology*, 138(2):165–172, 2020.
11. H Laviers and H Zambarakji. Enhanced depth imaging-oct of the choroid: a review of the current literature. *Graefe's Archive for Clinical and Experimental Ophthalmology*, 252:1871–1883, 2014.
12. Andrew G Lee, Thomas H Mader, C Robert Gibson, and William Tarver. Space flight–associated neuro-ocular syndrome. *JAMA ophthalmology*, 135(9):992–994, 2017.
13. Andrew G Lee, Thomas H Mader, C Robert Gibson, Tyson J Brunstetter, and William J Tarver. Space flight-associated neuro-ocular syndrome (sans). *Eye*, 32(7):1164–1167, 2018.
14. Andrew G Lee, Thomas H Mader, C Robert Gibson, William Tarver, Pejman Rabiei, Roy F Riascos, Laura A Galdamez, and Tyson Brunstetter. Spaceflight associated neuro-ocular syndrome (sans) and the neuro-ophthalmologic effects of microgravity: a review and an update. *npj Microgravity*, 6(1):7, 2020.
15. Stuart MC Lee, L Christine Ribeiro, David S Martin, Sara R Zwart, Alan H Feiveson, Steven S Laurie, Brandon R Macias, Brian E Crucian, Stephanie Krieger, Daniela Weber, et al. Arterial structure and function during and after long-duration spaceflight. *Journal of Applied Physiology*, 129(1):108–123, 2020.
16. Steven G Luke. Evaluating significance in linear mixed-effects models in r. *Behavior research methods*, 49:1494–1502, 2017.

17. Brandon R Macias, Nimesh B Patel, C Robert Gibson, Brian C Samuels, Steven S Laurie, Christian Otto, Connor R Ferguson, Stuart MC Lee, Robert Ploutz-Snyder, Larry A Kramer, et al. Association of long-duration spaceflight with anterior and posterior ocular structure changes in astronauts and their recovery. *JAMA ophthalmology*, 138(5): 553–559, 2020.
18. COL Thomas H Mader, C Robert Gibson, Michael Caputo, Norwood Hunter, Gerald Taylor, John Charles, and Richard T Meehan. Intraocular pressure and retinal vascular changes during transient exposure to microgravity. *American journal of ophthalmology*, 115(3):347–350, 1993.
19. Thomas H Mader, C Robert Gibson, and Andrew G Lee. Choroidal folds in astronauts. *Investigative Ophthalmology & Visual Science*, 57(2):592–592, 2016.
20. Xiao W Mao, Stephanie Byrum, Nina C Nishiyama, Michael J Pecaut, Vijayalakshmi Sridharan, Marjan Boerma, Alan J Tackett, Dai Shiba, Masaki Shirakawa, Satoru Takahashi, et al. Impact of spaceflight and artificial gravity on the mouse retina: biochemical and proteomic analysis. *International journal of molecular sciences*, 19(9):2546, 2018.
21. Yosbelkys Martin Paez, Lucy I Mudie, and Prem S Subramanian. Spaceflight associated neuro-ocular syndrome (sans): A systematic review and future directions. *Eye and Brain*, pages 105–117, 2020.
22. Javier Mazzaferri, Luke Beaton, Gisèle Hounye, Diane N Sayah, and Santiago Costantino. Open-source algorithm for automatic choroid segmentation of oct volume reconstructions. *Scientific reports*, 7(1):42112, 2017.
23. An L Moens, Hunter C Champion, Marc J Claeys, Barbara Tavazzi, Pawel M Kaminski, Michael S Wolin, Dirk J Borgonjon, Luc Van Nassauw, Azeb Haile, Muz Zviman, et al. High-dose folic acid pretreatment blunts cardiac dysfunction during ischemia coupled to maintenance of high-energy phosphates and reduces postreperfusion injury. *Circulation*, 117(14):1810–1819, 2008.
24. An L Moens, Christiaan J Vrints, Marc J Claeys, Jean-Pierre Timmermans, Hunter C Champion, and David A Kass. Mechanisms and potential therapeutic targets for folic acid in cardiovascular disease. *American Journal of Physiology-Heart and Circulatory Physiology*, 294(5):H1971–H1977, 2008.
25. Sarah Mrejen and Richard F Spaide. Optical coherence tomography: imaging of the choroid and beyond. *Survey of ophthalmology*, 58(5):387–429, 2013.
26. Joshua Ong, William Tarver, Tyson Brunstetter, Thomas Henry Mader, C Robert Gibson, Sara S Mason, and Andrew Lee. Spaceflight associated neuro-ocular syndrome: proposed pathogenesis, terrestrial analogues, and emerging countermeasures. *British Journal of Ophthalmology*, 107(7):895–900, 2023.
27. Arshi Parvaiz, Muhammad Anwaar Khalid, Rukhsana Zafar, Huma Ameer, Muhammad Ali, and Muhammad Moazam Fraz. Vision transformers in medical computer vision—a contemplative retrospection. *Engineering Applications of Artificial Intelligence*, 122: 106126, 2023.
28. Zarana S Patel, Tyson J Brunstetter, William J Tarver, Alexandra M Whitmire, Sara R Zwart, Scott M Smith, and Janice L Huff. Red risks for a journey to the red planet: The highest priority human health risks for a mission to mars. *npj Microgravity*, 6(1):33, 2020.
29. Diane N Sayah, Javier Mazzaferri, Pierre Ghesquière, Renaud Duval, Flavio Rezende, Santiago Costantino, and Mark R Lesk. Non-invasive in vivo measurement of ocular rigidity: clinical validation, repeatability and method improvement. *Experimental Eye Research*, 190:107831, 2020.
30. Diane N Sayah, Denise Descovich, Santiago Costantino, and Mark R Lesk. The association between the pulsatile choroidal volume change and ocular rigidity. *Ophthalmology Science*, page 100576, 2024.
31. Sumit Randhir Singh, Kiran Kumar Vupparaboina, Abhilash Goud, Kunal K Dansingani, and Jay Chhablani. Choroidal imaging biomarkers. *Survey of Ophthalmology*, 64(3): 312–333, 2019.
32. Marissé Masís Solano, Emmanuelle Richer, Farida Cheriet, Mark R Lesk, and Santiago Costantino. Mapping pulsatile optic nerve head deformation using oct. *Ophthalmology Science*, 2(4):100205, 2022.
33. Marissé Masís Solano, Charles Bélanger Nzakimuena, Rémy Dumas, Mark R Lesk, and Santiago Costantino. Ocular rigidity and choroidal thickness changes in response to microgravity: A case study. *American Journal of Ophthalmology Case Reports*, 32: 101940, 2023.
34. Marissé Masís Solano, Remy Dumas, Mark R Lesk, and Santiago Costantino. Ocular biomechanical responses to long-duration spaceflight. *IEEE Open Journal of Engineering in Medicine and Biology*, 2024.
35. Xiaodan Sui, Yuanjie Zheng, Benzheng Wei, Hongsheng Bi, Jianfeng Wu, Xuemei Pan, Yilong Yin, and Shaoting Zhang. Choroid segmentation from optical coherence tomography with graph-edge weights learned from deep convolutional neural networks. *Neurocomputing*, 237:332–341, 2017.
36. Hans Thisanke, Chamli Deshan, Kavindu Chamith, Sachith Seneviratne, Rajith Vidanaarachchi, and Damayanthi Herath. Semantic segmentation using vision transformers: A survey. *Engineering Applications of Artificial Intelligence*, 126:106669, 2023.
37. Ethan Waisberg, Joshua Ong, Mouayad Masalkhi, Kazuhito Shimada, and Andrew G Lee. Artificial gravity as a potential countermeasure for spaceflight associated neuro-ocular syndrome. *Eye*, pages 1–2, 2024.
38. Peter Wostyn, Charles R Gibson, and Thomas H Mader. Optic disc edema in astronauts from a choroidal point of view. *Aerospace Medicine and Human Performance*, 93(4): 396–398, 2022.
39. L Wu, M Masis, and E Hernandez-Bogantes. Choroidal imaging with spectral-domain optical coherence tomography, enhanced depth imaging may lead to a broader understanding of the pathogenesis of several eye diseases. *Retina Surgery Global Perspectives*, 114:39–42, 2011.
40. Enze Xie, Wenhai Wang, Zhiding Yu, Anima Anandkumar, Jose M Alvarez, and Ping Luo. Segformer: Simple and efficient design for semantic segmentation with transformers. *Advances in neural information processing systems*, 34:12077–12090, 2021.
41. Meng Xuan, Wei Wang, Danli Shi, James Tong, Zhuoting Zhu, Yu Jiang, Zongyuan Ge, Jian Zhang, Gabriella Bulloch, Guankai Peng, et al. A deep learning–based fully automated program for choroidal structure analysis within the region of interest in myopic children. *Translational Vision Science & Technology*, 12(3):22–22, 2023.
42. Haoran Zhang, Jianlong Yang, Ce Zheng, Shiqing Zhao, and Aili Zhang. Annotation-efficient learning for oct segmentation. *Biomedical Optics Express*, 14(7):3294–3307, 2023.
43. Sara R Zwart, C Robert Gibson, Thomas H Mader, Karen Ericson, Robert Ploutz-Snyder, Martina Heer, and Scott M Smith. Vision changes after spaceflight are related to alterations in folate-and vitamin b-12-dependent one-carbon metabolism. *The Journal of nutrition*, 142(3):427–431, 2012.
44. Sara R Zwart, Jesse F Gregory, Steven H Zeisel, Charles R Gibson, Thomas H Mader, Jason M Kinchen, Per M Ueland, Robert Ploutz-Snyder, Martina A Heer, and Scott M Smith. Genotype, b-vitamin status, and androgens affect spaceflight-induced ophthalmic changes. *The FASEB Journal*, 30(1):141, 2016.
45. Sara R Zwart, Charles R Gibson, Jesse F Gregory, Thomas H Mader, Patrick J Stover, Steven H Zeisel, and Scott M Smith. Astronaut ophthalmic syndrome. *FASEB Journal*, 31(9):3746–3756, 2017.

## Acknowledgements

Funding was provided by the Canadian Space Agency, the Canadian Institutes of Health Research, and the Fonds de Recherche en Ophtalmologie de l'Université de Montréal (FROUM). MMS received a scholarship from the Fonds de Recherche du Québec Santé. SC holds the Wolfe Professorship in Translational Research. We thank NASA and ESA for coordination and infrastructure.